Journal of Power Sources 195 (2010) 2346–2354

Contents lists available at ScienceDirect

Journal of Power Sources

journal homepage: www.elsevier.com/locate/jpowsour

# Exergy analysis of an integrated solid oxide fuel cell and organic Rankine cycle for cooling, heating and power production

Fahad A. Al-Sulaiman[a,*], Ibrahim Dincer[b], Feridun Hamdullahpur[c]

[a] Mechanical and Aerospace Engineering Department, Carleton University 1125 Colonel By Drive, Ottawa, Ontario, Canada K1S 5B6
[b] Faculty of Engineering and Applied Science, University of Ontario Institute of Technology 2000 Simcoe Street North, Oshawa, Ontario, Canada L1H 7L7
[c] Mechanical and Mechatronics Engineering Department, University of Waterloo, 200 University Avenue West, Waterloo, Ontario, Canada N2L 3G1

ARTICLE INFO

*Article history:*
Received 20 August 2009
Received in revised form 26 October 2009
Accepted 27 October 2009
Available online 6 November 2009

*Keywords:*
Trigeneration
Solid oxide fuel cell
Organic Rankine cycle
Energy
Exergy efficiency
Exergy destruction rate

ABSTRACT

The study examines a novel system that combined a solid oxide fuel cell (SOFC) and an organic Rankine cycle (ORC) for cooling, heating and power production (trigeneration) through exergy analysis. The system consists of an SOFC, an ORC, a heat exchanger and a single-effect absorption chiller. The system is modeled to produce a net electricity of around 500 kW. The study reveals that there is 3–25% gain on exergy efficiency when trigeneration is used compared with the power cycle only. Also, the study shows that as the current density of the SOFC increases, the exergy efficiencies of power cycle, cooling cogeneration, heating cogeneration and trigeneration decreases. In addition, it was shown that the effect of changing the turbine inlet pressure and ORC pump inlet temperature are insignificant on the exergy efficiencies of the power cycle, cooling cogeneration, heating cogeneration and trigeneration. Also, the study reveals that the significant sources of exergy destruction are the ORC evaporator, air heat exchanger at the SOFC inlet and heating process heat exchanger.



## 1. Introduction

Finding efficient power systems is of major concerns, especially with the depletion of fossil fuel sources with time. Energy demands are expected to keep increasing in the future. For instance, the world energy consumption is expected to increase to around 40% between 2006 and 2030 [1]. Thus, finding efficient systems is vital to reduce the unit of energy produced per the unit of fuel consumed. On the other hand, producing energy from fossil fuel causes some problem to the environment, such as global warming, air pollution, acid precipitation, ozone depletion, forest destruction and emission of radioactive substances, Dincer [2]. For example, from 1990 to 2007 the $CO_2$ equivalent emissions increased 17% in USA [3]. Therefore, finding efficient systems that produce less harmful emissions is crucial.

The efficiency of conventional power plants that are based on a single prime mover is usually less than 39%. That is, more than 60% of a plant's energy is lost. On the other hand, the overall efficiency of a conventional plant that produces electricity and heat separately is around 60% [4]. Alternatively, with the utilization of the waste heat from the prime mover, the efficiency of the trigeneration plants could reach 80% [4,5]. Also, the expected reduction in $CO_2$ emissions as a result of using trigeneration and cogeneration plants is 170 Mt year$^{-1}$ in 2015 while in 2030 the expected reduction is 950 Mt year$^{-1}$ [5].

Trigeneration is defined as the production of cooling, heating and power from the same source. In a trigeneration system, the waste energy from a generation unit, such as a gas turbine, is used to drive both the heating and cooling systems. Consequently, the use of a trigeneration plant results in an improvement of the total plant's efficiency and a reduction of the contamination to the environment. The degree of improvement of the plant is sensitive to the performance of each unit in the trigeneration plant and the approach of integrating the units of the plant.

Solid oxide fuel cells (SOFC) are considered an emerging technology as characterized by their high efficiency and low $CO_2$ emissions. An SOFC operates at high temperature and thus has high waste energy that can be integrated efficiently with a bottoming cycle. One of the potential systems that can be integrated with SOFC is organic Rankine cycle (ORC). ORC is similar to steam Rankine cycle; however, it uses organic working fluid instead of steam and requires less input heat to operate compared with steam Rankine cycle. SOFC and ORC are potential subsystems that can be used in trigeneration plants.

A number of studies have been conducted to examine the performance of a combined system of SOFC with a gas turbine [6–19]. Nevertheless, only a few studies have been conducted on the per-

* Corresponding author. Tel.: +1 613 520 2600x1833; fax: +1 613 520 5715.
*E-mail addresses:* fahadas@kfupm.edu.sa (F.A. Al-Sulaiman), Ibrahim.Dincer@uoit.ca (I. Dincer), fhamdull@uwaterloo.ca (F. Hamdullahpur).

0378-7753/$ – see front matter © 2009 Elsevier B.V. All rights reserved.
doi:10.1016/j.jpowsour.2009.10.075

**Nomenclature**

| | |
|---|---|
| $a$ | extent of steam reforming reaction for methane ($mol\,s^{-1}$) |
| $A$ | active surface area ($cm^2$) |
| $b$ | extent of water gas shift reaction ($mol\,s^{-1}$) |
| $c$ | extent of electrochemical reaction ($mol\,s^{-1}$) |
| $C$ | constant or heat capacity ($kW\,K^{-1}$) |
| $D_{aeff}$ | effective gaseous diffusivity through the anode ($cm^2\,s^{-1}$) |
| $D_{ceff}$ | effective gaseous diffusivity through the cathode ($cm^2\,s^{-1}$) |
| $F$ | Faraday constant ($C\,mol^{-1}$) |
| $\Delta G$ | change in specific molar Gibbs free energy ($J\,mol^{-1}$) |
| $ex$ | exergy per unit mass |
| $\overline{ex}_i^{ch}$ | chemical exergy |
| $ex^{ph}$ | physical exergy |
| $\dot{E}x_d$ | exergy destruction rate |
| $\dot{E}x_f$ | exergy of the fuel |
| $h$ | enthalpy ($kJ\,kg^{-1}$) |
| $I$ | current (A) |
| $j$ | current density ($A\,cm^{-2}$) |
| $j_{ac}$ | exchange current density of anode ($A\,cm^{-2}$) |
| $j_{sc}$ | exchange current density of cathode ($A\,cm^{-2}$) |
| $K$ | equilibrium constant |
| $L$ | thickness of an SOFC layer (cm) |
| $LHV$ | lower heating value ($kJ\,mol^{-1}$) |
| $m$ | mass (kg) |
| $N_{FC}$ | total number of fuel cells |
| $ORC$ | organic Rankine cycle |
| $\dot{Q}$ | heat rate (kW) |
| $R$ | universal gas constant ($J\,mol\,K^{-1}$) |
| $R_{contact}$ | resistivity contact |
| $r_{el,c}$ | electrical to cooling energy ratio |
| $r_{el,h}$ | electrical to heating energy ratio |
| $s$ | entropy ($kJ\,kg\,K^{-1}$) |
| $T$ | temperature (K) |
| $U_f$ | fuel utilization ratio |
| $U_{O_2}$ | air (oxidant) utilization ratio |
| $v$ | velocity ($m\,s^{-1}$) |
| V | volume ($m^3$) |
| $V$ | voltage (V) |
| $\dot{W}$ | power (kW) |
| $\dot{W}_{FC}$ | power of the fuel cell (W) |
| $x$ | molar concentration |
| $z$ | elevation |

*Greek letters*

| | |
|---|---|
| $\eta$ | efficiency |
| $\rho$ | electrical resistivity of cell components |

*Subscripts*

| | |
|---|---|
| *0* | atmospheric conditions |
| *a* | anode |
| *ac* | AC current |
| *act* | activation |
| *b*1 | blower 1 |
| *b*2 | blower 2 |
| *c* | cathode |
| *cog,c* | cooling cogeneration |
| *cog,h* | heating cogeneration |
| *conc* | concentration |
| *e* | electrolyte, exit |
| *el* | electrical power |
| *eq* | equilibrium |
| *ex* | exergy efficiency |
| *ev* | evaporator |
| *FC* | fuel cell |
| *h* | heating |
| *hp* | heating process |
| *in* | inlet |
| *int* | interconnect |
| *inverter* | DC to AC inverter |
| *g* | generator |
| *o* | organic |
| *oe* | ORC evaporator |
| *ohm* | ohmic |
| *op* | ORC pump |
| *ot* | ORC turbine |
| *N* | Nernst |
| *wgs* | water gas shift reaction |
| *sp* | solution pump |
| *tri* | trigeneration |
| *wp* | water pump |

*Superscripts*

| | |
|---|---|
| – | molar base |
| · | rate of a component |
| 0 | at standard pressure |

formance analysis of a combined SOFC with a gas turbine as a prime mover of trigeneration plants. A system of a combined SOFC with a gas turbine as prime mover of a trigeneration plant was analyzed by Burer et al. [20]. The study performed first and second law efficiencies of the potential on integrating a heat pump to the system. The study focused mainly on cost and $CO_2$ emission analysis using multi-criteria optimization. The optimization objectives were the annual total cost of power, heating and cooling generation and the annual $CO_2$ emissions rates. The study revealed that the system of a combined SOFC and gas turbine was an attractive economical and environmental solution when high electricity and natural gas prices were encountered. In a different study, an analysis of a hybrid system combining a microturbine and an SOFC as a prime mover of a trigeneration plant was carried out by Saito et al. [21]. The authors performed energy demand and consumption analyses of apartments, offices and hotels in Japan with the use of the hybrid system. The study revealed that the annual fuel consumption dropped by 32%, 36% and 42% for the apartments, offices and hotels, respectively.

A study that compared the electricity produced from a plant consisting of an integrated SOFC with an ORC or a microturbine was conducted by Verda [22]. The author showed that the integration of an SOFC with an ORC or a microturbine increases the plant electrical energy by 30%. However, the study focused on the pinch analysis of the heat exchangers in the systems that the author modeled. Also, the study did not include the integration of heating and cooling loads. Akkaya and Sahin [23] studied the energetic performance of a system that combined an SOFC with an ORC without any heating or cooling load. They found that the efficiency of the system increased by 14–25% for the system that combined the SOFC and ORC compared with the system that consists of SOFC only.

Al-Sulaiman et al. [24] conducted energy analysis of a trigeneration plant based on an SOFC and ORC. The study revealed that there was at least 22% gain in efficiency when a trigeneration system was used compared with only the power system. In another study, Al-Sulaiman et al. [25] examined the effect of changing the current density of the SOFC and SOFC size on the efficiency and

$CO_2$ emissions of a trigeneration plant based on an SOFC and ORC. The study revealed that the $CO_2$ emissions per MWh increases with increase in current density. Also, the study revealed that there was a considerable reduction of $CO_2$ emissions per MWh of trigeneration compared with only the power cycle.

In this study, a comprehensive exergy analysis of a trigeneration plant based on an SOFC and an ORC are conducted, and system exergy efficiencies and exergy destruction rates are then examined. These two parameters are examined under different variables, which include the current density of the SOFC, inlet flow temperature of the SOFC, turbine inlet pressure and ORC pump inlet temperature. This study shows how much improvement in the exergy efficiency when a trigeneration plant used compared with a thermal power conventional plant. Also, the study shows exergy destruction rate of different components of the system and the contribution of these components into exergy destruction. The system description and assumptions are presented next. Then, system modeling, results and discussion, and conclusions are presented, respectively.

## 2. System description

The proposed trigeneration system consists of an SOFC, an ORC, a heating process and a single-effect absorption chiller, as shown in Fig. 1. The waste heat from the SOFC is used to heat the organic fluid in the ORC. Consecutively, the waste heat from the ORC is used for heating and cooling. The waste heat from the ORC is used to produce steam in the heating process, using a heat exchanger and to produce cooling using a single-effect absorption chiller. To have an efficient ORC, the working fluid in the ORC should have a high critical temperature, so that a usable waste heat can be gained. One of the typical organic fluid types used to operate the ORC is n-octane, which has a relatively high critical temperature, 569 K. Hence, it is selected as the working fuel of the ORC.

## 3. Model development

The SOFC model and exergy analysis of the proposed system are presented in this section. The developed model is programmed using the Engineering Equation Solver (EES). The input data used in the code are given in Table 1. A number of assumptions were made to carry out the analysis. It was assumed that the system is at steady state and the pressure change is neglected except in the pumps, blowers, ORC turbine and valves. The assumptions for the SOFC model are [26]:

- Air that enters the SOFC consists of 79% $N_2$ and 21% $O_2$.
- Gas mixture at the exit of the fuel channel reaches at chemical equilibrium.
- Both air and fuel flows have the same temperature at the inlet to the SOFC.
- Both air and fuel flows have the same temperature at the exit of the SOFC.
- Radiation heat transfer between gas channels and solid structure is negligible.
- Contact resistances are negligible.

The energy analysis applied to the single-effect absorption chiller is similar to that used by Herold et al. [27]. The analysis of the single-effect absorption chiller is validated with [27]. The assumptions used to analyze the single-effect absorption chiller are [27]:

- The refrigerant is considered pure water (Sates 6–9).
- States 7, 10 and 13 are considered saturated liquid.
- State 9 is considered saturated vapor.
- The pressure in the desorber and condenser is considered equal.
- The pressure in the evaporator and the absorber is considered equal.

### 3.1. SOFC modeling

The selected fuel for the SOFC is methane. The chemical and electrochemical reactions that occur within the anode and cathode of the solid oxide fuel cell are:

$$CH_4 + H_2O \rightarrow CO + 3H_2 \quad (1)$$

$$CO + H_2O \rightarrow H_2 + CO_2 \quad (2)$$

$$H_2 + 1/2O_2 \rightarrow H_2O \quad (3)$$

**Table 1**
Input values to the system.

| | |
|---|---|
| ORC | |
| ORC turbine efficiency | 80% |
| ORC pump efficiency | 80% |
| Saturated liquid at the exit of the ORC condenser | |
| Effectiveness of the ORC evaporator | 80% |
| Baseline ORC pump pressure ratio | 100 |
| Mass flow rate | 0.95 kg $s^{-1}$ |
| Baseline turbine inlet pressure | 1600 kPa |
| ORC pump inlet temperature | 345 K |
| Electrical generator efficiency | 95% |
| Electrical motor efficiency | 95% |
| Chilling cycle | |
| Overall heat transfer coefficient of desorber | 70 kW $K^{-1}$ |
| Overall heat transfer coefficient of condenser | 80 kW $K^{-1}$ |
| Overall heat transfer coefficient of evaporator | 95 kW $K^{-1}$ |
| Overall heat transfer coefficient of absorber | 75 kW $K^{-1}$ |
| Effectiveness of solution heat exchanger | 70% |
| SOFC Colpan [26] | |
| DC–AC inverter efficiency | 95% |
| Fuel utilization factor | 0.85 |
| Active surface area | 100 $cm^2$ |
| Baseline current density | 0.75 A $cm^{-2}$ |
| Exchange current density of anode | 0.65 A $cm^{-2}$ |
| Exchange current density of cathode | 0.25 A $cm^{-2}$ |
| Effective gaseous diffusivity through the anode | 0.2 $cm^2$ $s^{-1}$ |
| Effective gaseous diffusivity through the cathode | 0.05 $cm^2$ $s^{-1}$ |
| Thickness of the anode | 0.05 cm |
| Thickness of the cathode | 0.005 cm |
| Thickness of the electrolyte | 0.001 cm |
| Thickness of the interconnect | 0.3 cm |
| Pressure of the cell | 101.3 kPa |
| Baseline inlet temperature to the SOFC | 1000 K |
| Bossel [28] | |
| $C1_e$ | 334 |
| $C2_e$ | −10,300 |
| $C1_a$ | 9.5 × 100,000 |
| $C2_a$ | −1,150 |
| $C1_c$ | 4.2 × 100,000 |
| $C2_c$ | −1,200 |
| $C1_{int}$ | 9.3 × 10,000 |
| $C2_{int}$ | −1,100 |
| Ambient condition | |
| Ambient temperature | 298.15 K |
| Ambient pressure | 101.3 kPa |
| Standard chemical exergy Szargut [31] | |
| $\overline{ex}^{ch,0}_{CH_4}$ | 831.6 kJ $mol^{-1}$ |
| $\overline{ex}^{ch,0}_{H_2O}$ | 9.5 kJ $mol^{-1}$ |
| $\overline{ex}^{ch,0}_{O_2}$ | 3.97 kJ $mol^{-1}$ |
| $\overline{ex}^{ch,0}_{N_2}$ | 0.72 kJ $mol^{-1}$ |
| $\overline{ex}^{ch,0}_{H_2}$ | 236.09 kJ $mol^{-1}$ |
| $\overline{ex}^{ch,0}_{CO_2}$ | 19.87 kJ $mol^{-1}$ |
| $\overline{ex}^{ch,0}_{O_2}$ | 275.1 kJ $mol^{-1}$ |

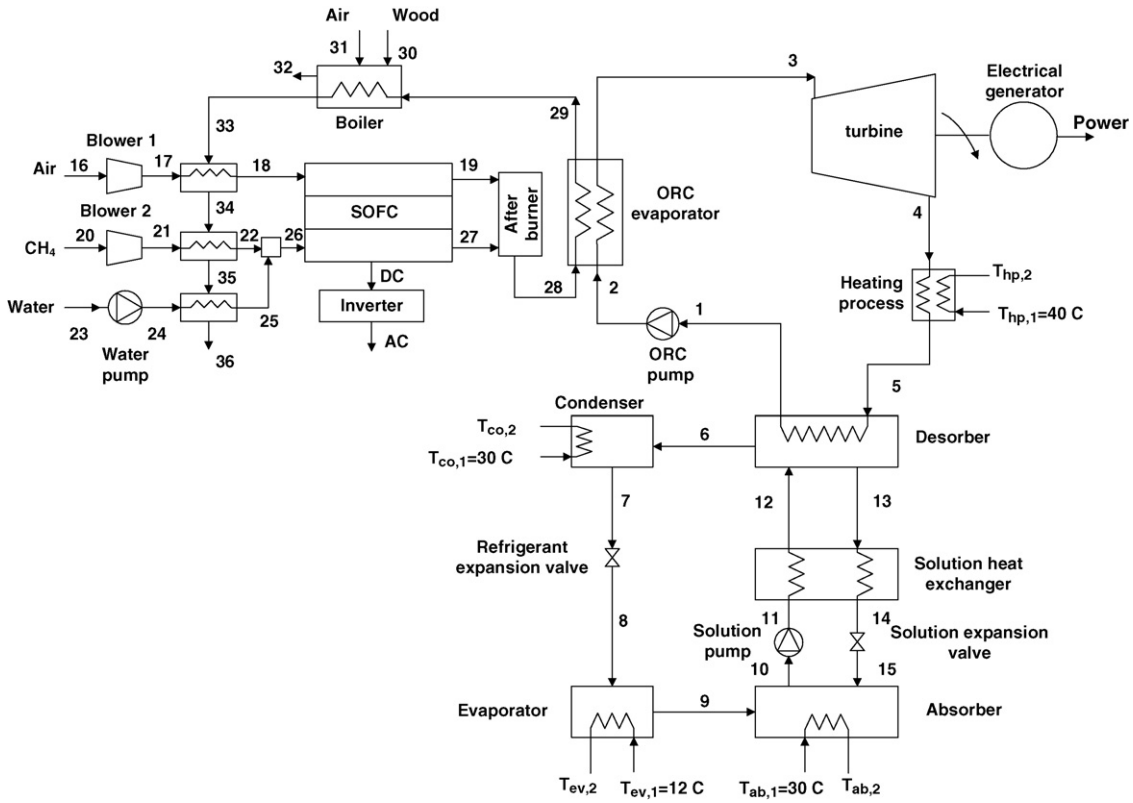


**Fig. 1.** Trigeneration plant with combined SOFC and organic Rankine cycle.

The cell voltage produced by the cell is the difference between the reversible cell voltage and the sum of the voltage loss. It is defined as

$$V_c = V_N - V_{loss} \tag{4}$$

where $V_c$, $V_N$ and $V_{loss}$ are cell voltage, reversible cell voltage and voltage loss, respectively. The equation of the reversible cell voltage is derived using Nernst equation and is defined as

$$V_N = -\frac{\Delta \bar{G}_f}{2F} - R\frac{T_{FC,exit}}{2F} \ln\left(\frac{x_{H_2O,27}}{x_{H_2,27}\sqrt{x_{O_2,19}}}\right) \tag{5}$$

where $G_f$ is the Gibbs free energy, $R$ is the universal gas constant (8.314 J (mol-K)$^{-1}$) and $F$ is Faraday constant (96,485 coulombs mol$^{-1}$). The voltage loss ($V_{loss}$) is the sum of three voltage losses that include the activation polarization, ohmic and concentration losses. It is defined as

$$V_{loss} = V_{ohm} + V_{act} + V_{cont} \tag{6}$$

where $V_{ohm}$ is defined by Bossel [28]; $V_{act}$ is defined by Kim [29]; and $V_{cont}$ is defined by Chan et al. [30] as follows:

$$V_{ohm} = (R_{contact} + \rho_a L_a + \rho_c L_c + \rho_{int} L_{int})j \tag{7}$$

$$V_{act} = V_{act,a} + V_{act,c} \tag{8}$$

$$V_{act,a} = \frac{RT_{FC,exit}}{F} \sinh^{-1}\left(\frac{j}{2j_{oa}}\right) \tag{9}$$

$$V_{act,c} = \frac{RT_{FC,exit}}{F} \sinh^{-1}\left(\frac{j}{2j_{oc}}\right) \tag{10}$$

$$V_{cont} = V_{cont,a} + V_{cont,c} \tag{11}$$

$$V_{cont,a} = -\frac{RT_{FC,exit}}{2F} \ln\left(1 - \frac{j}{j_{as}}\right) + \frac{RT_{FC,exit}}{2F} \ln\left(1 - \frac{P_{H_2,27}j}{P_{H_2O,27}j_{as}}\right) \tag{12}$$

$$V_{cont,c} = -\frac{RT_{FC,exit}}{4F} \ln\left(1 - \frac{j}{jcs}\right) \tag{13}$$

$$j_{as} = \frac{2FP_{H_2,27}D_{aeff}}{RT_{FC,exit}L_a} \frac{1}{1000,000[\text{cm}^3/\text{m}^3]} \tag{14}$$

$$j_{cs} = \frac{4FP_{O_2,19}D_{ceff}}{(P_0 - P_{O_2,19}/P_0)RT_{FC,exit}L_c} \frac{1}{1000,000[\text{cm}^3/\text{m}^3]} \tag{15}$$

where $\rho$ is the electrical resistivity of cell components, $L$ is the thickness of a cell component, $R_{contact}$ is the resistivity contact, $j$ is the current density, $j_{cs}$ is the exchange current density of cathode, $j_{as}$ is the exchange current density of anode, $D_{ceff}$ is the effective gaseous diffusivity through the cathode and $D_{aeff}$ is the effective gaseous diffusivity through the anode. The subscripts *ohm*, *act*, *cont*, *a*, *c*, *e* and *int* are ohmic, activation, concentration, anode, cathode, electrolyte and interconnect, respectively.

The electrical resistivity is defined as [28]

$$\rho_e = \left(C1_e \exp\left(\frac{C2_e}{T_{FC,exit}}\right)\right)^{-1} \tag{16}$$

$$\rho_a = \left(\frac{C1_a}{T_{FC,exit}} \exp\left(\frac{C2_a}{T_{FC,exit}}\right)\right)^{-1} \tag{17}$$

$$\rho_c = \left(\frac{C1_c}{T_{FC,exit}} \exp\left(\frac{C2_c}{T_{FC,exit}}\right)\right)^{-1} \tag{18}$$

$$\rho_{int} = \left(\frac{C1_{int}}{T_{FC,exit}} \exp\left(\frac{C2_{int}}{T_{FC,exit}}\right)\right)^{-1} \tag{19}$$

where $C1_e$–$C2_{int}$ are constants defined in [28] and shown in Table 1.

The model used to solve the equilibrium equations of the SOFC is based on a validated model developed by Colpan et al. [26], assuming the methane is fully converted. The molar conversion rates of Eqs. (1)–(3) are *a*, *b* and *c*, respectively. The molar flow rates of the

reaction equations, Eqs. (1)–(3), are derived next. The molar flow rates at the inlet of the air and fuel channels are defined as

$$\dot{n}_{O_2,18} = \dot{n}_{O_2,19} + \dot{n}_{O_2,u} \quad (20)$$

$$\dot{n}_{N_2,18} = \dot{n}_{N,19} \quad (21)$$

$$\dot{n}_{H_2O,26} = 2.5a \quad (22)$$

$$\dot{n}_{CH_4,26} = a \quad (23)$$

On the other side of the fuel cell, the molar flow rates at the exit of the air and fuel channels are defined as

$$\dot{n}_{O_2,19} = \frac{c}{2}\left(\frac{1}{U_{O_2}} - 1\right) \quad (24)$$

$$\dot{n}_{N_2,19} = \frac{79}{21}\left(\frac{c}{2U_{O_2}}\right) \quad (25)$$

$$\dot{n}_{H_2,27} = 3a + b - c \quad (26)$$

$$\dot{n}_{CO,27} = a - b \quad (27)$$

$$\dot{n}_{CO_2,27} = b \quad (28)$$

$$\dot{n}_{H_2O,27} = 1.5a - b + c \quad (29)$$

where the constant $c$ and the molar flow rate of the utilized oxygen, $\dot{n}_{O_2,u}$ are defined as

$$c = (3a + b)U_f \quad (30)$$

$$\dot{n}_{O_2,u} = \frac{c}{2} \quad (31)$$

The variables $\dot{n}$, $U_f$ and $U_{O_2}$ are molar flow rate, fuel utilization ratio and oxygen utilization ratio, respectively. The constants $a$ and $b$ are found using the equilibrium constant and current equations as defined below. The equilibrium constant is defined as

$$K_{wgs} = \exp\left(-\frac{\Delta G^0}{RT_{FC,exit}}\right) = \frac{x_{CO_2,27}x_{H_2,27}}{x_{CO,27}x_{H_2O,27}} \quad (32)$$

where $K_{wgs}$ is the waste gas shift equation and $x$ is the molar concentration.

The current and current density are defined respectively as

$$I = jA_a \quad (33)$$

$$j\frac{2Fc}{A_a} \quad (34)$$

where $I$ is the current and $A_a$ is the active surface area. The power of the fuel cell, $\dot{W}_{FC}$, is defined as

$$\dot{W}_{FC} = IV_c \quad (35)$$

### 3.2. Exergy analysis of the system

Unlike energy, exergy is not conserved. Exergy is defined as the maximum work that could be obtained from a system at a given state. Exergy destruction is an important parameter in exergy analysis. It is defined as the potential work lost due to irreversibility. The exergy destruction rate of a control volume for a steady state is defined as

$$\dot{E}_{x_d} = \sum_j \left(1 - \frac{T_0}{T_j}\right)\dot{Q}_j - \left(\dot{W}_{cv} - P_0\frac{dV_{cv}}{dt}\right) + \sum_i \dot{m}_i ex_i - \sum_e \dot{m}_e ex_e \quad (36)$$

where $T$, $P$, $V$, $ex$ and $\dot{E}_{x_d}$ are temperature, pressure, volume, exergy per mass flow rate and rate of exergy destruction, respectively. The subscript $i$ is the property value at state $i$ and the subscript 0 is the value of a property at the surrounding. The physical exergy per mass flow rate, $ex^{ph}$, at a given state is defined as

$$ex^{ph} = (h - h_0) - T_0(s - s_0) + \left(\frac{v^2 - v_0^2}{2}\right) + g(z - z_0) \quad (37)$$

where $h$, $s$, $v$, $g$ and $z$ are enthalpy per mass flow rate, entropy per mass flow rate, velocity, gravity and elevation, respectively. In this study, the velocity and elevation are neglected. On other hand, the chemical exergy of a single gas at a multi-gas mixture is defined as

$$\overline{ex}_i^{ch} = x_i\overline{ex}_i^{ch,0} + RT_0x_i \ \ln(x_i) \quad (38)$$

where $\overline{ex}_i^{ch,0}$ is the standard chemical exergy of a species in kJ mol$^{-1}$ as defined by Szargut [31] and listed in Table 1. The net power of the system is defined as

$$\dot{W}_{net} = \dot{W}_{FC,stack,ac} + \dot{W}_{ot}\eta_{motor} - \frac{\dot{W}_{op}}{\eta_{motor}} - \frac{\dot{W}_{sp}}{\eta_{motor}} - \frac{\dot{W}_{b1}}{\eta_{motor}} - \frac{\dot{W}_{b2}}{\eta_{motor}} - \frac{\dot{W}_{wp}}{\eta_{motor}} \quad (39)$$

where the subscripts $g$, $op$, $sp$, $b1$, $b2$ and $wp$ indicate generator, ORC pump, solution pump, blower one (air blower), blower two (methane blower) and water pump, respectively. The Greek letter, $\eta$, is the efficiency. The total exergy in the system is then defined as

$$\dot{E}_{x_{f,total}} = \dot{E}_{x_{f,CH_4}} + \dot{E}_{x_{f,wood}} \quad (40)$$

where $\dot{E}_{x_{f,total}}$, $\dot{E}_{x_{f,CH_4}}$ and $\dot{E}_{x_{f,wood}}$ are total exergy rate, exergy rate of methane at state 20 and exergy rate of wood at state 30, respectively. The exergy efficiency is defined as the ratio of the actual thermal efficiency to the maximum reversible thermal efficiency both under the same conditions. The exergy efficiency of the SOFC system is defined as

$$\eta_{ex,FC} = \frac{\dot{W}_{FC,stack,ac} - (\dot{W}_{b1}/\eta_{motor}) - (\dot{W}_{b2}/\eta_{motor}) - (\dot{W}_{wp}/\eta_{motor})}{E_{xf,CH_4}} \quad (41)$$

The exergy efficiency of the ORC is defined as

$$\eta_{ex,ORC} = \frac{\dot{W}_{ot}\eta_{motor} - (\dot{W}_{op}/\eta_{motor})}{\dot{E}_{x_{28}} - \dot{E}_{x_{29}}} \quad (42)$$

The net electrical exergy efficiency is defined as

$$\eta_{ex,et} = \frac{\dot{W}_{net}}{\dot{E}_{x_{f,total}}} \quad (43)$$

The cooling cogeneration exergy efficiency is defined as

$$\eta_{ex,cog,c} = \frac{\dot{W}_{net} + (1 - (T_0/T_{ev}))\dot{Q}_{ev}}{E_{x_{f,total}}} \quad (44)$$

where $\dot{Q}$ is the heat rate and the subscript $ev$ indicates the evaporator of the cooling cycle. The exergy efficiency of the heating cogeneration is defined as

$$\eta_{ex,cog,h} = \frac{\dot{W}_{net} + (1 - (T_0/T_{hp}))\dot{Q}_h}{\dot{E}_{x_{f,total}}} \quad (45)$$

where the subscripts $h$ and $hp$ indicate the heating and heating process heat exchanger. The exergy efficiency of the trigeneration is defined as

$$\eta_{ex,tri} = \frac{\dot{W}_{net} + (1 - (T_0/T_{ev}))\dot{Q}_{ev} + (1 - (T_0/T_{hp}))\dot{Q}_h}{\dot{E}_{x_{f,total}}} \quad (46)$$

where the subscript $tri$ indicates trigeneration.

## 4. Results and discussion

In this study, exergy efficiency and exergy destruction rate of the proposed trigeneration system are examined. The exergy efficiency and exergy destruction rate are examined under the variation of different variables. These variables are the current density of the SOFC, inlet flow temperature of the SOFC, pressure inlet of the turbine and inlet temperature of the ORC pump, $T_1$.

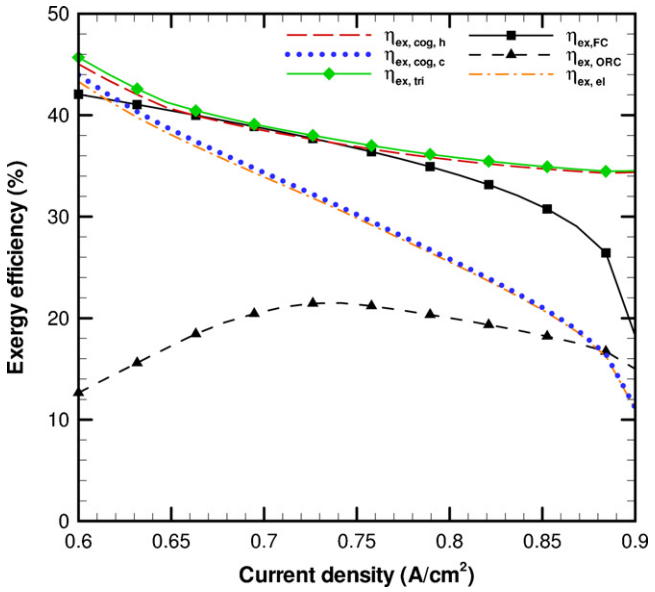


**Fig. 2.** Effect of the current density of the SOFC on exergy efficiency at $T_{FC,in}$ = 1000 K, $P_2$ = 1600 kPa, $T_1$ = 345 K.

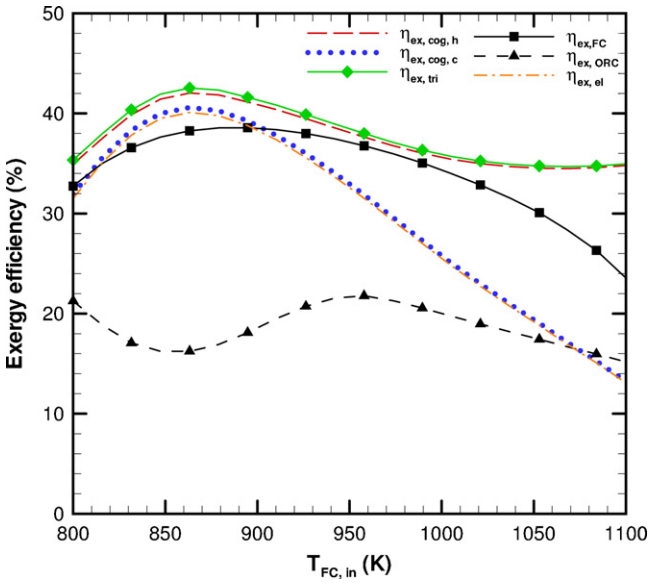


**Fig. 4.** Effect of SOFC inlet flow temperature on exergy efficiency at $j$ = 0.8 A cm$^{-2}$, $P_2$ = 1600 kPa, $T_1$ = 345 K.

### 4.1. Effect of current density of the SOFC

The effect of changing the current density of the SOFC on the exergy efficiency and exergy destruction rate is shown in Figs. 2 and 3, respectively. In Fig. 2, the net electrical exergy efficiency decreases as the current density increases. This reduction in the exergy efficiency is because of the decrease in the cell voltage as the current density increases and thus less power output from the SOFC as discussed in Al-Sulaiman et al. [24]. The highest net electrical exergy efficiency is 43% at a current density of 0.6 A cm$^{-2}$ and the lowest exergy efficiency is 11% at 0.9 A cm$^{-2}$. The cooling cogeneration exergy efficiency is 1% or less higher than the net electrical exergy efficiency. This small difference in the gained efficiency is because of the small amount of the cooling energy to the electrical energy in the cycle which is around 20% of the electrical energy. The heating cogeneration exergy efficiency decreases as the current density increases. The highest heating cogeneration exergy efficiency is 45% at a current density of 0.6 A cm$^{-2}$ and the lowest exergy efficiency is 34.5% at 0.9 A cm$^{-2}$. The trigeneration exergy efficiency is around 1% higher than the heating cogeneration exergy efficiency. This small difference in the efficiency is because of the small gain of the cooling cogeneration exergy efficiency compared with the net electrical exergy efficiency where trigeneration is defined as combined cooling, heating and power.

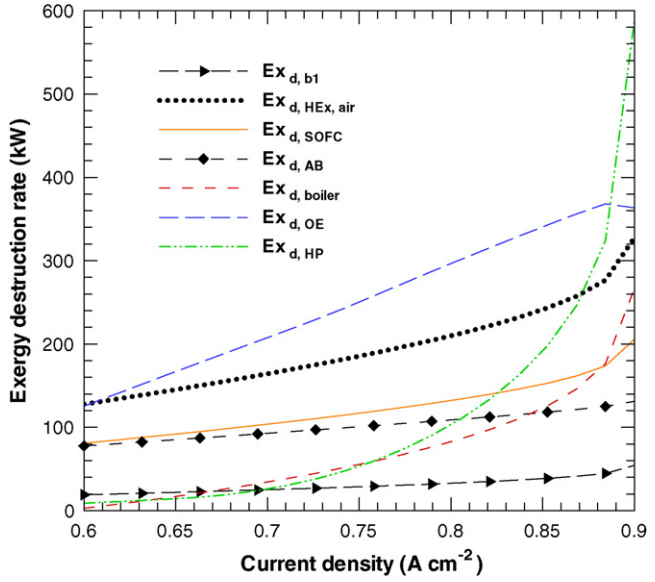


**Fig. 3.** Effect of SOFC current density on exergy destruction rate at $T_{FC,in}$ = 1000 K, $P_2$ = 1600 kPa, $T_1$ = 345 K.

The effect of changing the current density on the exergy destruction rate of different components of the system is shown in Fig. 3. Only the components of the system that show significant amount of exergy destruction rates are shown in the figure. It can be observed that all the exergy destruction components increases as the current density increases. The study reveals that the exergy destruction rates of blower 1 (air blower) and the after burner increases slightly as the current density increases. The amount of the change in the exergy destruction rate is less than 50 kW. On other hand, the change in the exergy destruction rate with current density is considerably more for the other components. This study shows that most of the exergy destructions occur at the ORC evaporator and air heat exchanger. However, at a high current density, the exergy destruction rate of the heating process heat exchanger is very high and reaches 580 kW at 0.9 A cm$^{-2}$. This significant increase in the exergy destruction rate of the heating process heat exchanger is because of the increase in the amount of the available waste heat for heating where the net electrical exegetic efficiency drops abruptly. The parametric study on the effect of the current density change on the exergy destruction rate suggests that further design improvement and optimization are needed to reduce the exergy destruction rate of the air heat exchanger, ORC evaporator and heating process heat exchanger.

### 4.2. Effect of the inlet flow temperature of the SOFC

The effect of changing the inlet flow temperature of the SOFC on the exergy efficiency and exergy destruction rate is shown in Figs. 4 and 5, respectively. In these two figures the temperature is studied from 800 to 1100 K. Fig. 4 shows that the change in the exergy efficiency as the inlet flow temperature change is different from that of the current density. The reason of this difference is because the cell voltage change differently with the inlet flow

temperature of the SOFC compared with the current density of the SOFC [24]. The study reveals that the temperature where the net electrical efficiency is the highest is the same temperature where the cooling cogeneration, heating cogeneration and trigeneration efficiencies are the highest. The reason of having the same temperature, where the highest efficiency is obtained, is because all of these four efficiencies are defined based on the chemical exergy of the fuel. Therefore, the highest efficiency is obtained at the same point where the most efficient combustion occurs. The physical exergy of the incoming fuel is zero since it enters into the system at atmospheric conditions. Fig. 5 shows the effect of changing the inlet flow temperature of the SOFC on the exergy destruction rate of different components of the system. The figure shows that the exergy destruction rates of the air blower and after burner are almost constant. Also, it can be noticed that the highest exergy destruction rate occurs at the air heat exchanger and ORC evaporator. Nevertheless, at a high inlet flow temperature the exergy destruction rate of the heating process heat exchanger is considerable. This abrupt increase in the exergy destruction rate of the heating process heat exchanger as the inlet flow temperature increases is associated with the increase in the amount of the waste heat as the net electrical efficiency drops.

### 4.3. Effect of the inlet pressure of the turbine

The effect of changing the inlet pressure of the turbine on the exergy efficiency and exergy destruction rate is shown in Figs. 6 and 7, respectively. In these figures the turbine inlet pressure is studied from 500 to 5000 kPa. It can be observed that the effect of changing the inlet pressure of the turbine on the efficiencies of the net electricity, cooling cogeneration, heating cogeneration and trigeneration is insignificant. The net electrical and cooling cogeneration exergy efficiencies increases 3% as the turbine inlet pressure increases, and heating cogeneration and trigeneration efficiencies increases 1%. On the other hand, the exergy efficiency of the ORC increases from 15% at 500 kPa to 22% at 5000 kPa. The exergy efficiency of the SOFC system is constant since it is independent of the change in turbine inlet pressure. The figure shows that as compared with the exergy efficiency of the power cycle there is on average a gain in exergy efficiency of 0.5% for cooling cogeneration, 10% for heating cogeneration and 11% for trigeneration.

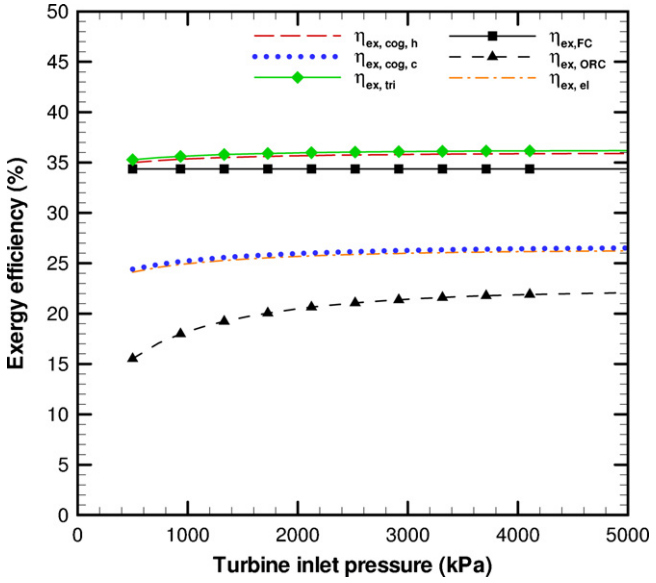


**Fig. 6.** Effect of turbine inlet pressure on exergy efficiency at $j = 0.8\,A\,cm^{-2}$, $T_{FC,in} = 1000\,K$, $T_1 = 345\,K$.

Fig. 7 shows that only the exergy destruction rate of the ORC evaporator and heating process heat exchanger varies with the change in the inlet pressure of the turbine. On the other hand, the other components of the system are constants since they are independent of the change in the turbine inlet pressure. The exergy destruction rate of the ORC evaporator decreases from 320 kW at 500 kPa to 280 kW at 5000 kPa while the exergy destruction rate of the heating process heat exchanger decreases from 120 kW at 500 kPa to 100 kW at 5000 kPa.

### 4.4. Effect of ORC pump inlet flow temperature

The effect of changing the ORC pump inlet flow temperature on the exergy efficiency and exergy destruction rate is shown in Figs. 8 and 9, respectively. In these figures the temperature is studied from 345 to 380 K. Fig. 8 shows that the change in the inlet temperature has an insignificant effect of the exergy efficiencies

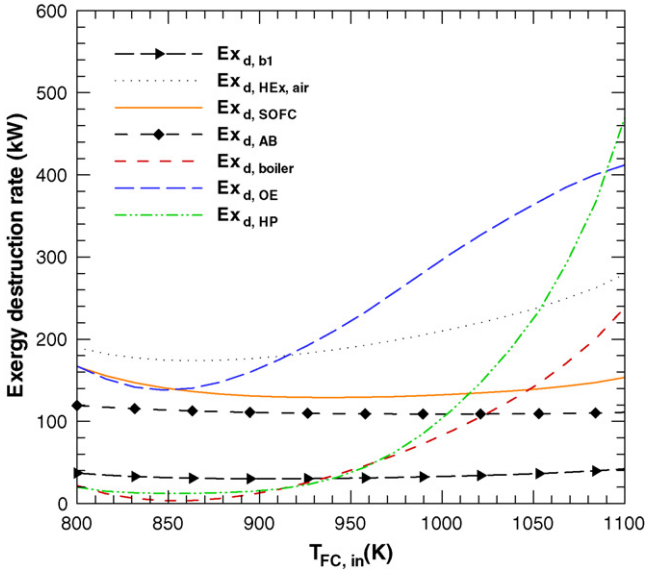


**Fig. 5.** Effect of SOFC inlet flow temperature on exergy destruction rate at $j = 0.8\,A\,cm^{-2}$, $P_2 = 1600\,kPa$, $T_1 = 345\,K$.

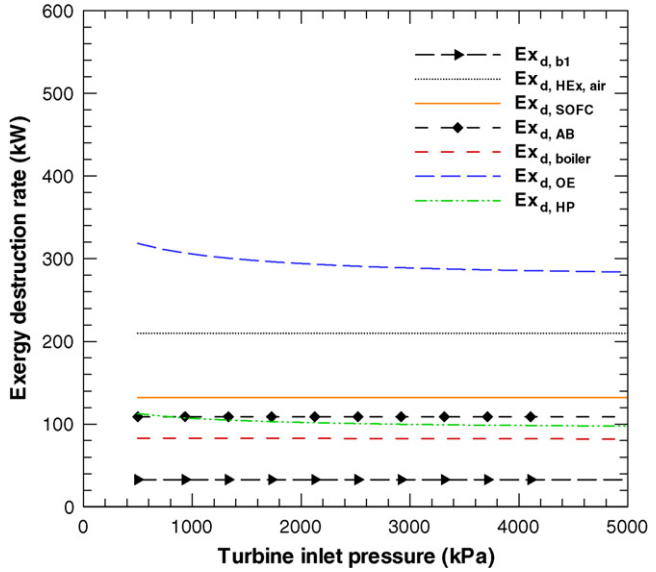


**Fig. 7.** Effect of turbine inlet pressure on exergy destruction rate at $j = 0.8\,A\,cm^{-2}$, $T_{FC,in} = 1000\,K$, $T_1 = 345\,K$.

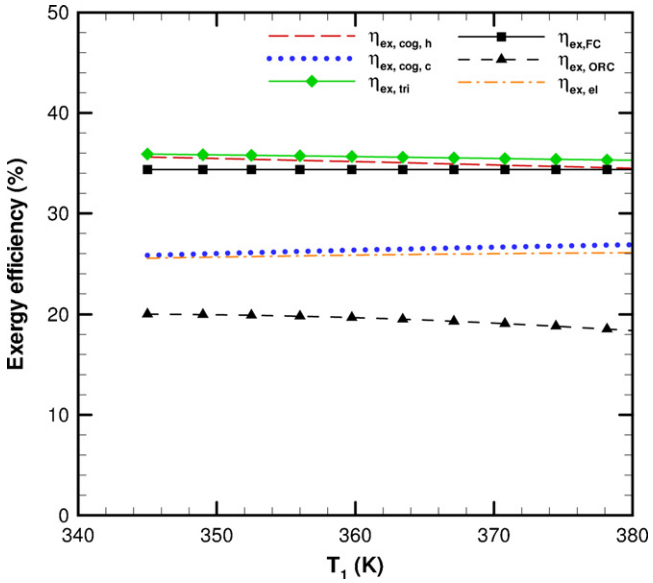


**Fig. 8.** Effect of organic Rankine cycle pump inlet temperature on exergy efficiency at $j = 0.8\ \mathrm{A\,cm^{-2}}$, $T_{FC,in} = 1000\ \mathrm{K}$, $P_2 = 1600\ \mathrm{kPa}$.

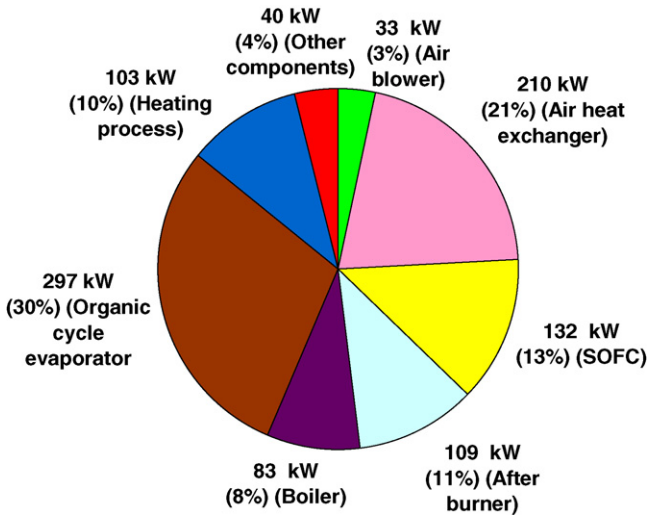


**Fig. 10.** Exergy destruction in kW and in percentage of the total exergy destructed for different trigeneration plant components at $j = 0.8\ \mathrm{A\,cm^{-2}}$, $T_{FC,in} = 1000\ \mathrm{K}$, $P_2 = 1600\ \mathrm{kPa}$, $T_1 = 345\ \mathrm{K}$.

of the power, cooling cogeneration, heating cogeneration and trigeneration. The exergy efficiency of the net electrical efficiency is around 25%. Using cooling cogeneration, the exegetic efficiency increases to 26% only. The reason of this small increase in the efficiency is the small size of the cooling energy to the electrical energy (1:5). On the other hand, exergy efficiency of heating cogeneration is around 35% and exergy efficiency of trigeneration is around 36%.

Fig. 9 shows that the exergy destruction rate of the ORC evaporator, boiler and heating process heat exchanger varies with the ORC pump inlet flow temperature. As the temperature increases, the exergy destruction rate of the ORC evaporator decreases. It decreases from 300 kW at 345 K to 240 kW at 380 K. This reduction in exergy destruction rate attributed to the less exergy difference available between the inlets and exits of the evaporator. Also, the study shows that there is an insignificant change in the exergy destruction rate of the boiler and heating process heat exchanger as the temperature increases.

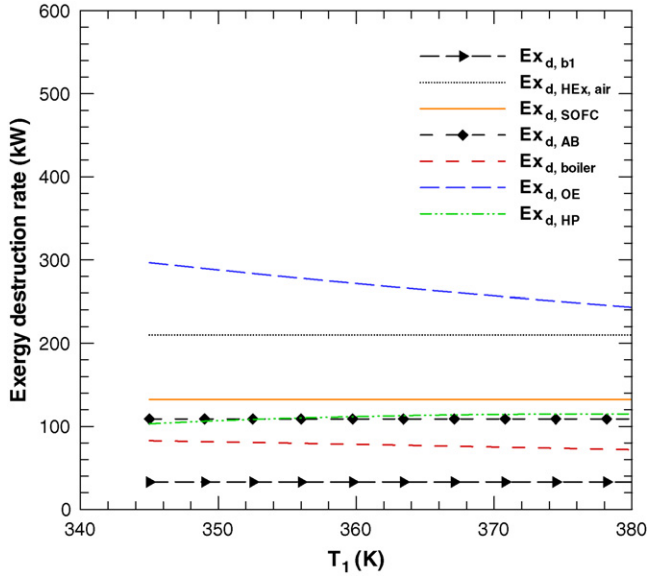


**Fig. 9.** Effect of organic Rankine cycle pump inlet temperature on exergy destruction rate at $j = 0.8\ \mathrm{A\,cm^{-2}}$, $T_{FC,in} = 1000\ \mathrm{K}$, $P_2 = 1600\ \mathrm{kPa}$.

### 4.5. Overall exergy destruction

The exergy destruction analysis of different components of the system at the baseline input data is shown in Fig. 10. The exergy destruction percentage that is shown in the figure is the percentage of the exergy destructed not the available exergy in the system. The exergy destruction analysis shows that 30% of the exergy destruction takes place in the ORC evaporator and 21% in the air heat exchanger at the inlet of the SOFC. The other components of the system that have high exergy destruction are SOFC (13%), after burner (11%), heating process heat exchanger (10%), biomass boiler (8%) and air blower (4%). Therefore, further improvement to the performance of these components is needed, specially the ORC evaporator and the air heat exchanger.

## 5. Conclusion

Exergy analysis of a combined SOFC and ORC system for cooling, heating and power production is conducted. The system is examined under the variation of the current density of the SOFC, inlet flow temperature of the SOFC, inlet pressure of the turbine and inlet temperature of the ORC pump. The main findings are:

- The exergy analysis of the trigeneration plant shows that the gain in the exergy efficiency when trigeneration is used compared with only power cycle is from 3 to 25%, depending on the operating condition.
- The exergy efficiencies of the power cycle, cooling cogeneration, heating cogeneration and trigeneration are insensitive to the change of the turbine inlet pressure and ORC pump inlet temperature.
- The most significant sources of exergy destruction rates are the ORC evaporator, air heat exchanger at the SOFC inlet and heating process heat exchanger. Therefore, further improvements in designing these three components are needed.
- The working fluid for the ORC is n-octane. Therefore, this conclusion is relatively limited to this fluid type.

## Acknowledgement

The first author acknowledges the financial support provided by King Fahd University of Petroleum and Minerals (KFUPM), Dhahran, Saudi Araiba, to carry out this research.

## References

[1] Energy Information Administration, International Energy Outlook, 2009.
[2] Ibrahim Dincer, Environmental impacts of energy, Energy Policy 27 (14) (1999) 845–854.
[3] U.S. Environmental Protection Agency, Inventory of U.S. Greenhouse Gas Emissions and Sinks: 1990–2007, 2009.
[4] Tom Kerr, Combined heating and power and emissions trading: options for policy makers, International Energy Agency (2008).
[5] International Energy Agency, Combined Heat and Power: Evaluating the Benefits of Greater Global Investment, 2008.
[6] Jens Palsson, Azra Selimovic, Lars Sjunnesson, Combined solid oxide fuel cell and gas turbine systems for efficient power and heat generation, Journal of Power Sources 86 (1–2) (2000) 442–448.
[7] S.H. Chan, H.K. Ho, Y. Tian, Multi-level modeling of sofc-gas turbine hybrid system, International Journal of Hydrogen Energy 28 (8) (2003) 889–900.
[8] Prapan Kuchonthara, Sankar Bhattacharya, Atsushi Tsutsumi, Energy recuperation in solid oxide fuel cell (sofc) and gas turbine (gt) combined system, Journal of Power Sources 117 (1–2) (2003) 7–13.
[9] TaeWon Song, Jeong Lak Sohn, Jae Hwan Kim, Tong Seop Kim, Sung Tack Ro, Kenjiro Suzuki, Performance analysis of a tubular solid oxide fuel cell/micro gas turbine hybrid power system based on a quasi-two dimensional model, Journal of Power Sources 142 (1–2) (2005) 30–42.
[10] Tae Won Song, Lak Sohn Jeong, Tong Seop Kim, Sung Tack Ro, Performance characteristics of a mw-class sofc/gt hybrid system based on a commercially available gas turbine, Journal of Power Sources 158 (1) (2006) 361–367.
[11] F. Calise, A. Palombo, L. Vanoli, Design and partial load exergy analysis of hybrid sofc-gt power plant, Journal of Power Sources 158 (1) (2006) 225–244.
[12] Jin Sik Yang, J.L. Sohn, Sung Tack Ro, Performance characteristics of a solid oxide fuel cell/gas turbine hybrid system with various part-load control modes, Journal of Power Sources 166 (1) (2007) 155–164.
[13] Pegah Ghanbari Bavarsad, Energy and exergy analysis of internal reforming solid oxide fuel cell-gas turbine hybrid system, International Journal of Hydrogen Energy 32 (17) (2007) 4591–4599.
[14] Mikhail Granovskii, Ibrahim Dincer, M.A. Rosen, Performance comparison of two combined sofc-gas turbine systems, Journal of Power Sources 165 (1) (2007) 307–314.
[15] Alexandros Arsalis, Thermoeconomic modeling and parametric study of hybrid sofc-gas turbine-steam turbine power plants ranging from 1.5 to 10 mwe, Journal of Power Sources 181 (2) (2008) 313–326.
[16] Pilar Lisbona, L.M. Romeo, Enhanced coal gasification heated by unmixed combustion integrated with an hybrid system of sofc/gt, International Journal of Hydrogen Energy 33 (20) (2008) 5755–5764.
[17] Ali Volkan Akkaya, Bahri Sahin, Hasan Huseyin Erdem, An analysis of sofc/gt chp system based on exergetic performance criteria, International Journal of Hydrogen Energy 33 (10) (2008) 2566–2577.
[18] Y. Haseli, I. Dincer, G.F. Naterer, Thermodynamic modeling of a gas turbine cycle combined with a solid oxide fuel cell, International Journal of Hydrogen Energy 33 (20) (2008) 5811–5822.
[19] Tak-Hyoung Lim, Rak-Hyun Song, Dong-Ryul Shin, Jung-Il Yang, Heon Jung, I.C. Vinke, Soo-Seok Yang, Operating characteristics of a 5 kW class anode-supported planar sofc stack for a fuel cell/gas turbine hybrid system, International Journal of Hydrogen Energy 33 (3) (2008) 1076–1083.
[20] M. Burer, K. Tanaka, D. Favrat, K. Yamada, Multi-criteria optimization of a district cogeneration plant integrating a solid oxide fuel cell-gas turbine combined cycle, heat pumps and chillers, Energy 28 (6) (2003) 497–518.
[21] Motohiro Saito, Hideo Yoshida, yuhei Iwamoto, Akio Ueda, An analysis of a micro cogeneration system composed of solid oxide fuel cell, microturbine, and $H_2O$/libr absorption refrigerator, Journal of Thermal Science and Technology 2 (2) (2007) 168–179.
[22] Vittorio Verda, Solid oxide fuel cell system configurations for distributed generation, Journal of Fuel Cell Science and Technology 5 (4) (2008).
[23] Ali Volkan Akkaya, Bahri Sahin, A study on performance of solid oxide fuel cell-organic Rankine cycle combined system, International Journal of Energy Research 33 (6) (2009) 553–564.
[24] Fahad A. Al-Sulaiman, Ibrahim Dincer, Feridun Hamdullahpur, Energy analysis of a trigeneration plant based on solid oxide fuel cell and organic Rankine cycle, International Journal of Hydrogen Energy, in press, doi:10.1016/j.ijhydene.2009.09.047.
[25] F.A. Al-Sulaiman, Feridun Hamdullahpur, Ibrahim Dincer, Efficiency and environmental impact assessments of a trigeneration plant using sofc and orc, in: Global Conference on Global Warming, Istanbul, Turkey, 2009, 11 pp.
[26] Can Ozgur Colpan, Ibrahim Dincer, Feridun Hamdullahpur, Thermodynamic modeling of direct internal reforming solid oxide fuel cells operating with syngas, International Journal of Hydrogen Energy 32 (7) (2007) 787–795.
[27] K.E. Herlod, R. Radermacher, S.A. Klein, Absorption Chillers and Heat Pumps, CRC Press, 1996.
[28] U.G. Bossel, Final Report on SOFC Data Facts and Figures, Swiss Federal Office of Energy, 1992.
[29] Jai-Woh Kim, A.V. Virkar, Kuan-Zong Fung, K. Mehta, S.C. Singhal, Polarization effects in intermediate temperature, anode-supported solid oxide fuel cells, Journal of the Electrochemical Society 146 (1) (1999) 69–78.
[30] S.H. Chan, C.F. Low, O.L. Ding, Energy and exergy analysis of simple solid-oxide fuel-cell power systems, Journal of Power Sources 103 (2) (2002) 188–200.
[31] J. Szargut, Exergy Method Technical and Ecological Applications, WIT Press, 2005.